DOI: 10.1002/chem.200901929

Thermally Stable Porous Hydrogen-Bonded Coordination Networks Displaying Dual Properties of Robustness and Dynamics upon Guest Uptake

Ji-Jun Jiang,[a] Lei Li,[a] Mei-Hua Lan,[a] Mei Pan,[a] Andreas Eichhöfer,[b] Dieter Fenske,[b] and Cheng-Yong Su*[a]

Abstract: Two series of microporous lanthanide coordination networks of the general formula, $\{[Ln(ntb)Cl_3]\cdot x H_2O\}_n$ (series **1**: monoclinic $C2/c$, Ln = Sm and Tb; series **2**: hexagonal $P3_1/c$, Ln = Sm and Eu; ntb = tris(benzimidazol-2-ylmethyl)amine, $x = 0$–4) have been synthesized and characterized by IR, elemental analyses, thermal gravimetry, and single-crystal and powder X-ray diffraction methods. In both series, the monomeric $[Ln(ntb)Cl_3]$ coordination units are consolidated by N–H···Cl or C–H···Cl hydrogen bonds to sustain three-dimensional (3D) networks. However, the different modes of hydrogen bonding in the two series lead to crystallization of the same $[Ln(ntb)Cl_3]$ monomers in different forms (monoclinic vs. hexagonal), consequently giving rise to distinct porous structures. The resulting hydrogen-bonded coordination networks display high thermal stability and robustness in water removal/inclusion processes, which was confirmed by temperature-dependent single-crystal-to-single-crystal transformation measurements. Adsorption studies with H_2, CO_2, and MeOH have been carried out, and reveal distinct differences in adsorption behavior between the two forms. In the case of MeOH uptake, the monoclinic network shows a normal type I isotherm, whereas the hexagonal network displays dynamic porous properties.

Keywords: coordination networks · host–guest systems · hydrogen bonds · lanthanides

Introduction

The design and syntheses of supramolecular coordination architectures have attracted tremendous attention over the past decades due to their potential applications in the fields of magnetism, catalysis, sensing, porous materials, and nonlinear optical activity.[1] Microporous crystal structures are of particular interest because they may have commercial potential in gas storage or separation.[2] To achieve this goal, one essential crystal engineering strategy is to obtained thermally stable and robust metal-organic frameworks (MOFs) that display permanent porosity after removal of the guest molecules.[1–3] The rigid three-dimensional (3D) MOFs formed from stiff bridging ligands[1,4] have proven to represent one good structural approach to achieving this goal. Meanwhile, assembly of suitably hydrogen-bonded networks (HB networks) could become an alternative promising approach.[5]

On the other hand, it has been realized that the very large pores within a MOF might ultimately be detrimental for gas storage purposes, and that even the porosity might not be essential for gas storage capacity of the solids.[3a,b] Recent research in MOFs has shown that the flexibility of the framework could be of fundamental significance to the guest adsorption/desorption processes.[6] Crystal structures without pores can acquire gas storage capability through structural transformations upon guest uptake.[3a] Moreover, such flexibility may endow these structures with dynamics that are responsive to external stimuli (such as heat, pressure, guest molecules), thus generating more novel functions as "smart" materials.[7]

So far, a number of flexible microporous MOFs based on metal–ligand dative bonds have been found,[8] but rational design of a crystal structure calculated to possess dynamic

[a] J.-J. Jiang, L. Li, M.-H. Lan, M. Pan, Prof. C.-Y. Su
MOE Laboratory of Bioinorganic and Synthetic Chemistry
State Key Laboratory of Optoelectronic Materials and Technologies
School of Chemistry & Chemical Engineering
Sun Yat-Sen University, Guangzhou 510275 (China)
Fax: (+86) 20-8411-5178
E-mail: cesscy@mail.sysu.edu.cn

[b] Dr. A. Eichhöfer, Prof. D. Fenske
Institut für Nanotechnologie, Forschungszentrum Karlsruhe
Postfach 3640, 76021 Karlsruhe (Germany)

Supporting information for this article is available on the WWW under http://dx.doi.org/10.1002/chem.200901929.

properties largely remains a challenge. If, however, it is taken into account that organic hydrogen-bonded networks have long been extensively studied with regard to flexibility in the solid state, due to their weaker interactions,[9] combinations of dative bonds and hydrogen bonds (HBs) in the construction of hydrogen-bonded coordination networks could represent a promising route for soft porous materials (see Scheme S1 in the Supporting Information).[10] The thus generated porous hydrogen-bonded coordination networks might be able to display bifunctional properties, such as robustness and dynamics, that might potentially have better adaptability to external stimuli than MOFs based solely on dative bonds.

Here we report two series of hydrogen-bonded coordination networks containing 1D channels for guests inclusion: namely $\{[Ln(ntb)Cl_3]\cdot x H_2O\}_n$ as shown in Scheme 1, below (series **1**: monoclinic *C*2/*c*, Ln = Sm and Tb; series **2**: hexagonal $P3_1/c$, Ln = Sm and Eu. ntb = tris-(benzimidazol-2-ylmethyl)amine, $x = 0$–4). The same $[Ln(ntb)Cl_3]$ coordination subunits were hydrogen-bonded in different ways: N–H···Cl and C–H···Cl hydrogen bonds gave monoclinic networks in series **1**, whereas N–H···Cl HBs forming hexagonal networks dominated in series **2**. The polymorphism of the crystal structures results in distinct gas adsorption capabilities. Although both series feature high thermal stabilities and robust HB networks, the hexagonal networks display dynamic porosity upon MeOH uptake, demonstrating the dual functions of robustness and dynamics in these hydrogen-bonded coordination networks.

Results and Discussion

Preparation, characterization, and polymorphism: All the complexes are readily available by direct treatment of the hydrated lanthanide chloride $LnCl_3\cdot 9H_2O$ with ntb ligand, offering the same monomeric $[Ln(ntb)Cl_3]$ coordination motif (Scheme 1). However, different crystals were formed, depending on the reaction systems. Upon diffusion of diethyl ether into CH_3OH solutions, the crystals crystallized in a monoclinic system (**1-Sm**·$x H_2O$ and **1-Tb**·$x H_2O$), whereas upon slow evaporation of CH_3OH/THF mixtures (4:1 v/v) the crystals crystallized in a hexagonal system (**2-Sm**·$x H_2O$ and **2-Eu**·$x H_2O$). All complexes have been characterized by elemental analysis and IR spectroscopy. The phase purities of the bulk samples have been checked by powder X-ray diffraction (PXRD), which shows close matches of the measured patterns with simulated ones obtained from the single-crystal data (see below).

The water molecules contained in the crystals seem to be susceptible to the crystallization conditions. When the crystals were left open to air, slow partial escape of water molecules from the crystals occurred, and when the crystals were heated, all water molecules could be completely removed. This caused discrepancies in water molecule contents analyzed for crystal or bulk samples at different times. After complete removal of all solvate water molecules, **1-Sm** and **1-Tb** (or **2-Sm** and **2-Eu**) can be regarded as isomorphous complexes,[11] whereas **1-Sm** and **2-Sm** can be viewed as polymorphic crystals.[12] For the hydrated complexes, however, the lattice water molecules in monoclinic series **1** and hexagonal series **2** are variable; this make it equivocal to describe two series as polymorphic forms, even though they have the same $[Ln(ntb)Cl_3]$ coordination motifs (but different packing modes; vide infra).[13] To avoid ambiguity with nomenclature, we choose the hydrated **1-Sm**·$2H_2O$ and **2-Sm**·$2H_2O$ complexes—which contain the same lattice water molecule pattern—simplified as their dehydrated forms **1-Sm** and **2-Sm** as representatives for discussion.

Crystal structures and packing modes: The single-crystal data for **1-Sm**·$2H_2O$, **2-Eu**·$3H_2O$, and **2-Sm**·$2H_2O$ were collected (Table 1, below), whereas the **1-Tb**·$2H_2O$ complex was only verified by space group determination as isostructure to **1-Sm**·$2H_2O$. The structural analyses also confirmed the isostructures of **2-Eu**·$3H_2O$ and **2-Sm**·$2H_2O$. Both in the **1-Sm**·$2H_2O$ and in the **2-Sm**·$2H_2O$ structures, the central Sm^{3+} ions are seven-coordinated by four N atoms from the tetradentate ntb ligand and three Cl^- anions as shown in Figure 1a, giving rise to the same neutral and discrete $[Sm(ntb)Cl_3]$ coordination unit. The ntb ligand features a tripodal coordination mode with three benzimidazole (Bim) arms forming a propeller host to catch hold of the central Sm^{3+} ion, leaving three NH groups on one side as HB donors and three Cl^- anions on the other side as HB acceptors. Selected interatomic distances and angles are listed in Table S1 in the Supporting Information. The Ln–N distances in **1-Sm** and **2-Sm** are comparable, similarly to those in analogous Ln^{3+} complexes.[14]

The crystal packing analyses revealed that HBs play important roles in directing arrangements of the $[Sm(ntb)Cl_3]$ units in the crystal lattice (Table S2 in the Supporting Information).

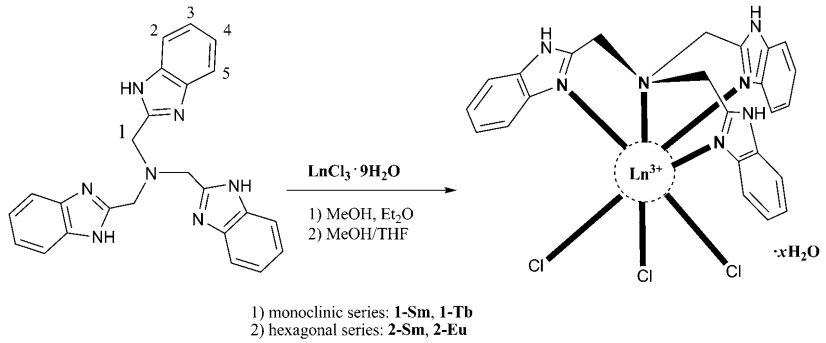

Scheme 1. Structure of the ntb ligand and syntheses of complexes.

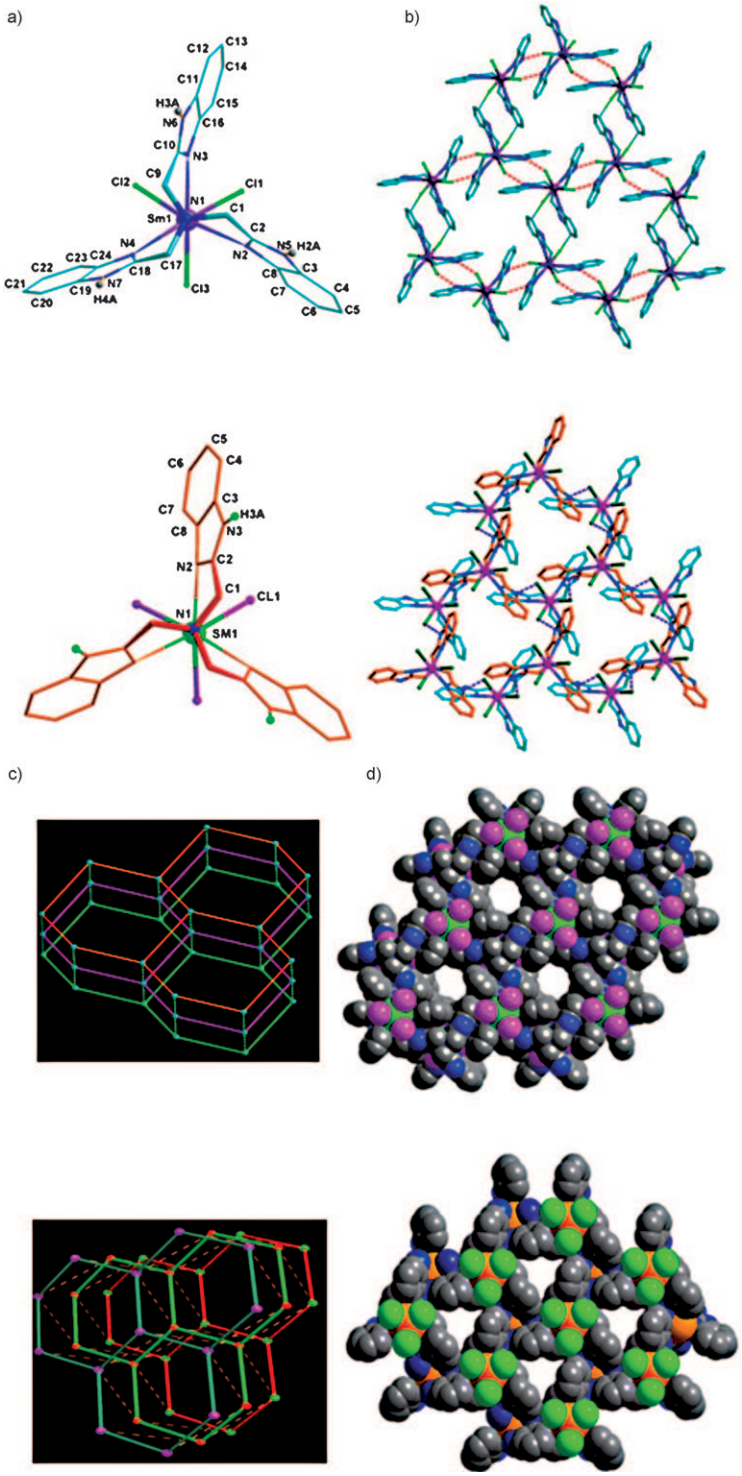

Figure 1. Crystal structures of complexes **1-Sm** (upper) and **2-Sm** (lower): a) molecular structures showing the coordination geometries of the Sm^{3+} ions in the $[Sm(ntb)Cl_3]$ motifs, b) 2D layers formed from hydrogen bonds shown in dashed lines, c) 3D networks sustained by hydrogen bonds between 2D layers showing packing mode in simplified 6^3 net topology, and d) the cylindrical and triangular channels formed in the *c* direction shown in space-filling mode (guest molecules are omitted for clarity).

In principle, besides three −NH HB donors and three Cl^- HB acceptors, each $[Sm(ntb)Cl_3]$ unit can also provide −CH sites acting as potential HB donors.[15] As depicted in Figure 1b, the three Cl^- anions of each $[Sm(ntb)Cl_3]$ unit in **1-Sm** form two N−H···Cl HBs and one C−H···Cl HB with their side-by-side $[Sm(ntb)Cl_3]$ neighbors. These HBs link $[Sm(ntb)Cl_3]$ units alternately in the opposite direction to generate a honeycomb 2D layer in the *ab* plane, where intermolecular π–π interactions (3.52 Å) between adjacent Bim rings are in evidence. In addition, three Cl^- anions form three more C−H···Cl HBs with three methylene H atoms of the head-to-tail $[Sm(ntb)Cl_3]$ neighbors (Figure S1 in the Supporting Information). These HBs direct the $[Sm(ntb)Cl_3]$ units so that they align exactly along the *c*-axis, causing an overlap crystal packing of the 2D layers as shown in simplified fashion in Figure 1c.

In contrast, in **2-Sm** the three Cl^- anions of each $[Sm(ntb)Cl_3]$ unit form three crystallographically equivalent N−H···Cl HBs with three different $[Sm(ntb)Cl_3]$ neighbors. These HBs join the $[Sm(ntb)Cl_3]$ units into a double layer extending in the *ab* plane (Figure 1b). If we also consider such a double layer as a 2D network, an offset crystal packing of double layers along the *c*-axis is obvious, as can be seen in Figure 1c.

Therefore, in both **1-Sm** and **2-Sm** overall 3D hydrogen-bonded coordination networks have been assembled. However, the difference in the formation of HBs leads to polymorphic forms from the same $[Sm(ntb)Cl_3]$ building units. In **1-Sm** the overlap packing of the 2D layers results in a monoclinic network containing cylindrical channels (effective pore diameter 4.8 Å) encircled by six Bim rings, whereas in **2-Sm** the offset packing of the 2D layers gives rise to a hexagonal network featuring triangular channels (effective pore diameter 4.0 Å) encircled by three Bim rings (Figure 1d). The guest water molecules are encapsulated inside these channels, accounting for 22.1% of the potential solvent-accessible area in **1-Sm** and 22.7% in **2-Sm**, as calculated by PLATON.[16] Although the disorder of the water molecules prevents exact analyses of their HB interactions, aggregation of water molecules as clusters in **1-Sm** and as polymers in **2-Sm** can clearly be seen in Figure S1 in the Supporting Information. It is noticeable that all three −NH donors and Cl acceptors in **2-Sm** are involved in hydrogen-bonding interactions between $[Sm(ntb)Cl_3]$ units, whereas in **1-Sm** only two −NH donors are involved. The remaining −NH donor in **1-Sm** forms O−H···N HBs with the guest water molecules. These differences should influence the guest uptake behavior (see below). On the other hand, the absence of one N−H···Cl HB in **1-Sm** in relation to **2-Sm** seems to be compensated for by formation of weaker C−H···Cl HBs and π–π interactions. This may be the reason why polymorphism can easily occur when the same $[Sm(ntb)Cl_3]$ units crystallize under slightly different solvent systems.

Thermal stability and single-crystal-to-single-crystal guest water de/rehydration: Thermal gravimetric analysis (TGA) and variable-temperature powder X-ray diffraction (VT-PXRD) were performed to examine the thermal stabilities

and robustness of the microporous networks upon removal of the water guests. TGA curves were recorded for freshly prepared bulk samples of **1-Sm** and **2-Sm** in the 25 to 700 °C temperature range (Figure S2 in the Supporting Information). Sample **1-Sm** displays a gradual weight loss (5.0 %) up to 220 °C, corresponding to the loss of two water molecules per Sm^{3+} (calculated 5.1 %). In contrast, sample **2-Sm** shows a slow weight loss before 150 °C and then a rapid one between 150 and 200 °C, totaling 10.1 %, amounting to four water molecules per Sm^{3+} (calculated 9.9 %). Complete removal of solvate water molecules at the relatively high temperature may be related to the aggregation of water molecules within the channels and the small channel apertures discussed above. To examine the rehydration ability of the dehydrated **2-Sm**, the sample was treated in the following ways and again subjected to TGA measurements. 1) The fresh sample was heated to 220 °C and maintained at this temperature for half an hour, 2) the sample was allowed to cool to room temperature in air, or 3) the dehydrated sample was directly dipped in water. As shown in Figure S2 in the Supporting Information, the dehydrated sample was only able to adsorb one water molecule per Sm^{3+} (2.5 %) when allowed to cool in air, but when the sample was dipped in water, rehydration by more than four water molecules per Sm^{3+} could be observed (13.0 %).

The VT-PXRD measurements further confirmed that the networks are robust with respect to dehydration. It is clear from Figure 2 and from Figures S3 and S4 in the Supporting

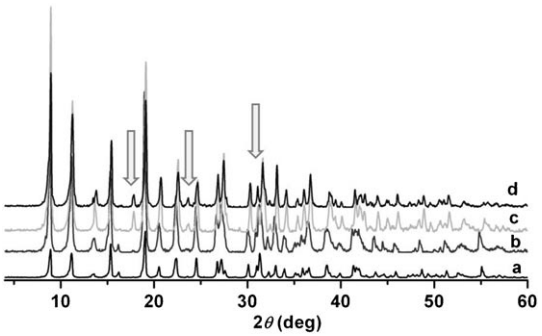

Figure 2. VT-PXRD patterns of **2-Sm** bulk sample at: a) 28, b) 130, c) 160, and d) 340 °C.

Information that the diffraction profiles of **1-Sm** remain unchanged up to 380 °C, at which the diffraction intensity starts to decrease (Figure S3 in the Supporting Information). This indicates that the microporosity in **1-Sm** is retained at this temperature and that the HB network remains intact after removal of the guest water molecules. The VT-PXRD patterns of **2-Sm** (Figure S4 in the Supporting Information) reveal that the crystalline sample became amorphous when heated to about 400 °C. Below this temperature, the microporous network is maintained. It is notable from Figure 2 that a peak at $2\theta = 16.2°$ weakens upon dehydration. Instead, two new peaks appear at $2\theta = 17.7$ and 23.5°. In addition, the peaks in the high 2θ region are moved slightly. These observations clearly denote that the chemical content in the unit cell is changed upon heating and that the network is slightly shrunk after the removal of the guest water molecules.[17]

Conclusive evidence of the robustness of the network with respect to guest evacuation was provided by the single-crystal-to-single-crystal study on re/dehydration of the same crystal. After collection of reflection data on a single crystal of **2-Sm**·2 H_2O, the same crystal was heated in situ to 160 °C (433 K) and 200 °C (473 K) and was then allowed to cool in air to 20 °C (293 K). The single crystallinity was found to be retained well during the variable-temperature measurements and the corresponding reflecting data were collected, to allow the assignment of **2-Sm** [433 K], **2-Sm** [473 K], and **2-Sm** [473–293 K] (Table 2, below). The structural analyses confirmed that in all cases the [Sm(ntb)Cl_3] coordination motifs and their overall crystal packing modes remained unchanged at the different temperatures. However, the guest water molecules inside the channels had been removed nearly completely at 160 °C and completely at 200 °C, as evidenced by the small electron residua of 0.774 and 0.534 e $Å^{-3}$, respectively, in the final refinements. As the completely dehydrated crystal cooled from 200 to 20 °C in air, one water per Sm^{3+} was readsorbed, which was verified by the satisfactory refinement of the data set from **2-Sm** [473–293 K] and is also consistent with the TGA results discussed above. On the other hand, the cell dimensions of the crystal at the different temperatures and before/after removal of water molecules are slightly changed. The potential solvent-accessible voids calculated by PLATON for **2-Sm** (22.7 %), **2-Sm** [473 K] (17.4 %), and **2-Sm** [473–293 K] (23.6 %) also vary slightly. These results suggest that the HB network in **2-Sm** is somewhat flexible, shrinking or expanding slightly with de/rehydration, in agreement with the observation of the peak shift from the VT-PXRD measurements and corroborated by the exact co-relation of the measured and simulated PXRD patterns (Figure S5 in the Supporting Information).

From above discussion we can see that the networks in both **1-Sm** and **2-Sm** feature high thermal stability and robust microporosity. The detailed re/dehydration behavior study on the **2-Sm** crystals revealed that the desorption and readsorption of the guest water molecules could take place in a reversible single-crystal-to-single-crystal manner as shown in Scheme S2 in the Supporting Information. Moreover, the evacuated porous network can capture different amounts of water guests under different conditions, implying good tolerance and adaptability towards guest uptake.

Solvent and gas adsorption: The complexes **1-Sm** and **2-Sm** were tested for solvent guest adsorption in the following procedures: 1) drying of the samples at 180 °C under vacuum for 12 h, 2) dipping of the dehydrated samples into the solvents for 48 h, 3) filtering out and washing of the dipped samples with anhydrous ethyl ether for three times, followed by drying in the infrared oven for 12 h, and 4) ^1H NMR investigation. The following solvent systems

were selected: 1) benzene, 2) chloroform, 3) a chloroform/acetone mixture (95:5 v/v), and 4) a benzene/acetone mixture (9:1 v/v). From Figure S6 in the Supporting Information we can see that **1-Sm** can only adsorb benzene, whereas **2-Sm** is able to adsorb both benzene and acetone. It is a surprise that the polar solvent chloroform could not be adsorbed either by **1-Sm** or by **2-Sm**, whereas **2-Sm** has a strong preference for acetone over chloroform but equal preference for acetone and benzene, evidenced by competitive adsorption tests in the chloroform/acetone (95:5 v/v) and benzene/acetone (9:1 v/v) mixtures. With regard to the channel environments, the cylindrical cavity in **1-Sm** and the triangular cavity in **2-Sm**, both surrounded by Bim rings, might facilitate inclusion of the nonpolar benzene guest, whereas the voids formed in between the $[Sm(ntb)Cl_3]$ layers may enable inclusion of polar guest. However, the differences in channel size and shape in **1-Sm** and **2-Sm** seems to impose selectivity on adsorption of guest molecules. The PXRD measurements verify that the microporous networks in **1-Sm** and **2-Sm** show no significant change after the guest solvents are adsorbed.

The gas and vapor adsorption behavior of the networks of **1-Sm** and **2-Sm** were investigated with N_2, CO_2, H_2, and MeOH. The as-synthesized samples (weight 50–100 mg) were dried under high vacuum at 120 °C for 24 h to remove water molecules prior to measurements. The adsorption isotherms of N_2 measured at 77 K for **1-Sm** and **2-Sm** indicated that only surface adsorption had occurred, suggesting that nitrogen molecules cannot diffuse into the channels at this temperature. In contrast, the adsorption isotherms of CO_2 measured at 195 K exhibited similar type I-like profiles, but revealed that **1-Sm** and **2-Sm** display distinctly different capacities for CO_2 storage. As shown in Figure 3a, **1-Sm** has a low CO_2 adsorption capacity of only 13.6 $mL\,g^{-1}$, amounting to 0.4 CO_2 molecules per metal ion, whereas **2-Sm** shows a relatively larger capacity for CO_2, adsorbing a maximum of 45.1 $mL\,g^{-1}$ CO_2 at 1 atm and room temperature, corresponding to 1.3 CO_2 molecules per metal ion. Uptakes of H_2 in **1-Sm** and **2-Sm** were measured at 77 K under high pressures of up to 100 bar (Figure 3b). It is worth noting that **1-Sm** and **2-Sm** possess comparable capacities for H_2 storage at high pressure, reaching 1.1% for **1-Sm** and 1.0% for **2-Sm**, corresponding to 3.6 and 3.3 H_2 molecules per metal ion, respectively. At low pressure, however, **1-Sm** is able to adsorb H_2 more rapidly than **2-Sm**, indicative of distinguishable H_2 uptake kinetics between **1-Sm** and **2-Sm**. In general, both **1-Sm** and **2-Sm** display typical guest uptake behavior characteristic of rigid MOFs possessing robust microporosity[1] both for CO_2 and for H_2. Although the adsorption and desorption processes are not completely reversible, as can be seen from the CO_2 isotherms in Figure 3a, no drastic adsorption jump was observed. This implies that only slight network "breathing"[1] takes place upon gas uptake, similar to that discussed above for de/rehydration.

In contrast, the adsorption isotherms for MeOH vapor measured at 298 K for **1-Sm** and **2-Sm** exhibit significantly different features, as can be seen in Figure 3c. Although the maximum amounts of MeOH adsorbed by **1-Sm** and **2-Sm** at 1 atm are comparable—114.8 and 132.9 $mg\,g^{-1}$, corresponding to 2.4 and 2.8 MeOH molecules per metal ion for **1-Sm** and **2-Sm**, respectively—the guest uptakes in **1-Sm** and

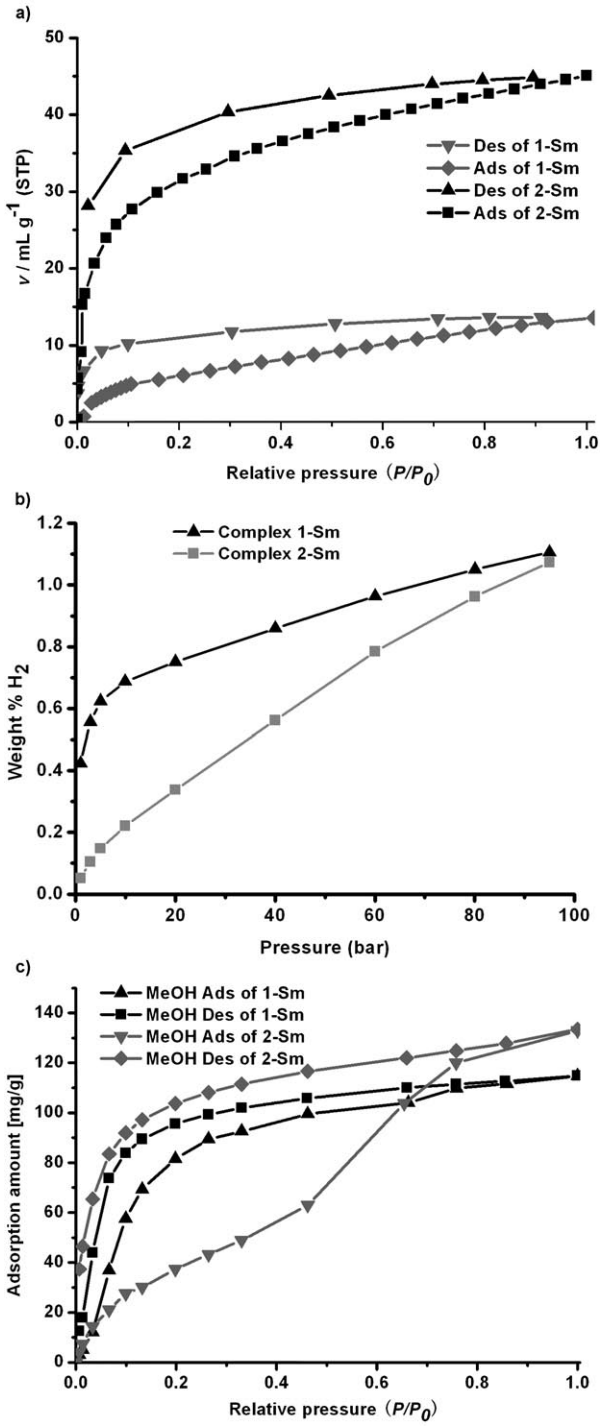

Figure 3. a) Gas (CO_2) adsorption/desorption isotherms at 195 K for **1-Sm** and **2-Sm** after activation at 120 °C for 24 h. b) Gas (H_2) adsorption properties of **1-Sm** and **2-Sm** at 77 K after activation at 120 °C for 24 h. c) MeOH vapor adsorption/desorption isotherms at 298 K for **1-Sm** and **2-Sm** after degassing for 24 h at 120 °C.

2-Sm show clearly different behavior: **1-Sm** displays normal type I isotherms whereas **2-Sm** exhibits a remarkable hysteresis loop between adsorption and desorption. Adsorption of MeOH in **1-Sm** rapidly reaches a plateau at about $P/P_o = 0.1$, whereas **2-Sm** adsorbs MeOH slowly before $P/P_o = 0.4$. After this pressure, adsorption of MeOH increases rapidly. This means that there is a drastic structural transformation induced by MeOH uptake in **2-Sm**,[18] characteristic of dynamic microporosity exhibited by flexible MOFs.[1] Such differences in MeOH vapor desorption/adsorption processes may originate from the differences in channel sizes and shapes between the networks of **1-Sm** and **2-Sm**. The **2-Sm** network has relatively smaller pore diameters (4.0 vs 4.8 Å) than **1-Sm** and a more confined channel environment (triangular vs. cylindrical), so the occurrence of more significant network dynamics for **2-Sm** upon MeOH uptake than for **1-Sm** is understandable.

The above results suggest that the network in **2-Sm**, besides the characteristics of high thermal stability and robustness that it shares with **1-Sm**, also features a dual property as shown in Scheme 2: namely, robustness and dynamics with respect to interactions with different guests molecules. Upon uptake of H_2O, CO_2, or H_2 guest molecules, **2-Sm** mainly displays network robustness, but upon uptake of MeOH guests, **2-Sm** can also show network dynamics. Although dual character of rigidity and flexibility has already been found in dative-bonded MOFs,[19] networks sustained by weaker hydrogen-bonding interactions may have advantages over the dative MOFs: 1) structural modulation may become easier, as exemplified by the facile polymorphism between **1-Sm** and **2-Sm**, and 2) dynamic responses to external stimuli are simpler to implement owing to the more "flexible" networks.

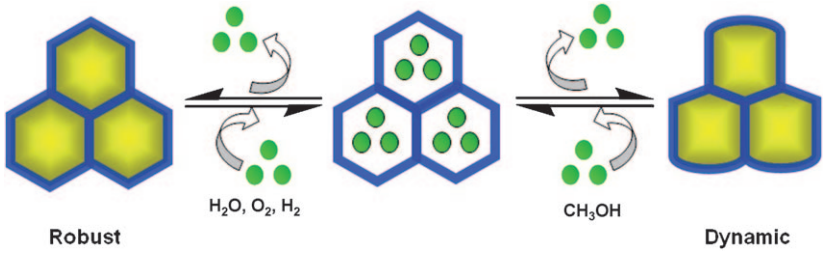

Scheme 2. Schematic representation of dual-property character with respect to different guest uptake in **2-Sm**.

Photophysical properties: UV and photoluminescence spectra were recorded for **1-Tb** and **2-Eu** at room temperature. UV spectroscopy shows that **1-Tb** and **2-Eu** have similar absorptions in MeOH solution, each displaying two bands around 275 and 282 nm, whereas in the solid state they each show a broad band with a maximum at about 290 nm and a shoulder at about 350 nm (Figure S7 in the Supporting Information). These absorption bands resemble those of the ntb ligand and are assignable to intraligand π–π* transitions.[20]

The luminescence spectra of **1-Tb** and **2-Eu** in the solid state, with excitation at 290 nm, display characteristic Ln^{3+} f–f emissions as depicted in Figure S8 in the Supporting Information. The **1-Tb** complex shows the expected sequence of $^5D_4 \rightarrow {}^7F_J$ transitions ($J = 6$, 5, 4 or 3) without further splitting. The most intense band at 583 nm is assigned to the $^5D_4 \rightarrow {}^7F_4$ transition, whereas the other three peaks at 492, 548, and 624 nm are attributed to $^5D_4 \rightarrow {}^7F_6$, $^5D_4 \rightarrow {}^7F_5$, and $^5D_4 \rightarrow {}^7F_3$ transitions, respectively.[16,20b] The **2-Eu** complex shows salient emission peaks at 592, 611, and 615 nm, which are contributed by $^5D_0 \rightarrow {}^7F_1$ and $^5D_0 \rightarrow {}^7F_2$ transitions. In addition, a small peak at 580 nm originating from the $^5D_0 \rightarrow {}^7F_0$ transition appears. Observation of this emission, together with the fact that the $^5D_0 \rightarrow {}^7F_2$ emission is stronger than the $^5D_0 \rightarrow {}^7F_2$ emission, indicates that the Eu^{3+} ion lies in a non-centrosymmetric coordination site,[20b] consistently with the structural analysis results.

Conclusion

In summary, two series of 3D microporous hydrogen-bonded coordination networks have been constructed from the same $[Ln(ntb)Cl_3]$ monomers containing both HB donors and acceptors. Self-assembly of the discrete $[Ln(ntb)Cl_3]$ monomers through N–H···Cl or C–H···Cl HBs leads to the crystallization of polymorphic networks under slightly different conditions. 1D channels of distinct size and shape, in which solvent guests and gases can be adsorbed, are formed in the polymorphic crystals. In general the HB networks feature in high thermal stabilities up to 350 °C and robustness against removal of the guest molecules, which have been verified by the study on re/dehydration by the TGA, VT-PXRD, and SCSC structural analysis methods. The investigation of the adsorption of solvents and gases indicates that the polymorphic HB networks show adsorption selectivity towards solvent guests such as benzene, acetone, and chloroform, together with differentiating gas-uptake behavior with N_2, CO_2, H_2, and MeOH. Dynamic microporosity has been observed for MeOH adsorption/desorption, implying that the HB networks might represent a potential structural model possessing dual properties of robustness and dynamics.

Experimental Section

Physical methods: Solvents and starting materials were purchased commercially and were used without further purification unless otherwise noted. Hydrated lanthanide chlorides were prepared from the corre-

sponding oxides. The ligand tris(2-benzimidazolylmethyl)amine (ntb) was synthesized by a slight modification of the method of Phillips by Oki et al.[21] in a yield of 72%. Infrared spectra were measured with a Nicolet/Nexus 670 FT-IR spectrometer with KBr pellets. The X-ray powder diffraction was recorded with a Rigaku D/Max-2200 diffractometer at 40 kV, 40 mA with a Cu-target tube and a graphite monochromator. Thermogravimetric analyses (TGA) were performed in air under 1 atm pressure at a heating rate of 10 °C min^{-1} with a Perkin–Elmer/TGS-2 analyzer. Emission spectra were obtained with a Combined Fluorescence Lifetime and Steady State FLS920 spectrometer. UV spectra were obtained with a UV 3150 UV spectrophotometer. The adsorption isotherms for MeOH were measured with an IGA 003 series instrument (Hiden Isochema, Ltd.). The adsorption isotherms of CO_2 were measured with BELmax 00027 adsorption equipment (BEL Japan). The high-pressure hydrogen storage capability was evaluated at 77 K with a RUBOTHERM magnetic suspension balance (Ankersmid, B.V., the Netherlands). Before the measurements, the samples were evacuated under dynamic vacuum at 120 °C for 24 h to remove the included solvent molecules.

Preparation of {[Ln(ntb)Cl$_3$]·xH$_2$O}$_n$ (series 1): A solution of ntb (40 mg, 0.1 mmol) in hot methanol (3 mL) was carefully mixed with a solution of $LnCl_3 \cdot 9H_2O$ (0.1 mmol) in methanol (1 mL). After filtration, slow diffusion of ethyl ether into the mixture over 24 h afforded colorless crystals. Yield: 42 mg, 64.7%. Dehydrated **1-Sm**: IR (KBr): $\tilde{\nu}$ = 3089(w), 2103(w), 1601(m), 1529(w), 1491(w), 1218(s), 1009(w), 807(w), 624(m) and 658(w); elemental analysis (%) calcd for $SmC_{24}H_{21}N_7Cl_3$: C 43.40, H 3.19, N 14.76; found: C 43.50, H 3.43, N 14.97. Hydrated **1-Tb**·2H$_2$O: IR (KBr): $\tilde{\nu}$ = 3084(w), 2107(w), 1598(m), 1527(w), 1493(w), 1216(s), 1007(w), 811(w), 621(m), 655(w) cm^{-1}; elemental analysis (%) calcd: C 40.67, H 3.56, N 13.83%; found: C 40.15, H 4.06, N 12.97%.

Preparation of {[Ln(ntb)Cl$_3$]·xH$_2$O}$_n$ (series 2): A solution of ntb (40 mg, 0.1 mmol) in hot methanol (4 mL) was carefully mixed with a solution of $LnCl_3 \cdot 9H_2O$ (0.1 mmol) in THF (1 mL). After filtration, the mixture was left untouched in a sealed test tube. Colorless single crystals had formed within 12 h under ambient conditions. Yield: 61 mg, 89.6%. Hydrated **2-Sm**·3H$_2$O: IR (KBr): $\tilde{\nu}$ = 3342(s), 3087(w), 2103(w), 1598(m), 1529(w), 1491(w), 1218(s), 1007(w), 807(w), 624(m), 658(w) cm^{-1}; elemental analysis (%) calcd for $SmC_{24}H_{27}N_7Cl_3O_3$: C 40.13, H 3.79, N 13.65; found: C 39.93, H 4.17, N 13.06. Hydrated **2-Eu**·3H$_2$O: IR (KBr): $\tilde{\nu}$ = 3337(s), 3079(w), 2104(w), 1596(m), 1527(w), 1493(w), 1219(s), 1005(w), 805(w), 626(m), 655(w) cm^{-1}; elemental analysis (%) calcd for $EuC_{24}H_{27}N_7Cl_3O_3$: C 40.04, H 3.78, N 13.62; found: C 40.23, H 4.06, N 14.18.

Crystal structure determination: The diffraction reflections were collected with a four-circle Enraf–Nonius CAD4 diffractometer ($Mo_{K\alpha}$ radiation, λ = 0.71073 Å) at 293 K for **1-Sm**·2H$_2$O, and with a Bruker SMART Apex CCD system with graphite-monochromated $Mo_{K\alpha}$ radiation (λ = 0.71073 Å) at 293 K for **2-Eu**·3H$_2$O. Structures were solved by direct methods followed by difference Fourier syntheses, and were then refined by full-matrix, least squares techniques on F^2 with SHELXL.[22] All the non-hydrogen atoms were refined with anisotropic parameters whereas H atoms were placed in calculated positions and refined with use of a riding model. The H atoms on the solvated water molecules were not added. For the **2-Sm**·2H$_2$O complex, variable-temperature single-crystal X-ray diffraction analyses were performed with the same crystal. The intensity data were recorded with an Oxford Gemini S Ultra CCD diffractometer with graphite-monochromated Mo-Kα radiation (λ = 0.71073 Å). The data collection was started first at 293 K with an as-prepared sample (**2-Sm**·2H$_2$O), and then with heating to 433 K (**2-Sm** [443 K]), continuously to 473 K (**2-Sm** [473 K]), and finally decreasing to 293 K (**2-Sm** [473–293 K]). The crystallinity of the sample was maintained well during the temperature cycle, and the structures were refined satisfactorily. Crystallographic data and refinement parameters are listed in Tables 1 and 2. Selected interatomic distances and angles are listed in Table S1 in the Supporting Information.

CCDC-737404, 737405, 737406, 737407, 737408, and 737409 contain the supplementary crystallographic data for this paper. These data can be obtained free of charge from The Cambridge Crystallographic Data Centre via www.ccdc.cam.ac.uk/data_request/cif.

Table 1. Crystallographic data for **1-Sm**, **2-Eu**, and **2-Sm**.

	1-Sm·2H$_2$O	**2-Eu**·3H$_2$O	**2-Sm**·2H$_2$O
empirical formula	$C_{48}H_{48}Cl_6N_{14}O_4Sm_2$	$C_{24}H_{27}C_{13}EuN_7O_3$	$C_{24}H_{25}C_{13}N_7O_2Sm$
formula weight	1398.40	719.84	700.21
space group	*C*2/*c*	*P*31*c*	*P*31*c*
crystal system	monoclinic	hexagonal	hexagonal
a [Å]	25.9769(10)	11.5227(5)	11.4971(6)
b [Å]	14.2025(10)	11.5227(5)	11.4971(6)
c [Å]	16.0804(10)	12.9540(12)	13.0502(5)
α [°]	90	90	90
β [°]	94.642(10)	90	90
γ [°]	90	120	120
V [Å^3]	5913.2(6)	1489.51(17)	1493.91(12)
Z	4	2	2
ρ_{calcd} [g cm^{-3}]	1.571	1.605	1.528
T [K]	293(2)	293(2)	293(2)
μ [mm^{-1}]	2.29	2.412	2.224
GOF	1.026	1.024	1.033
R_{int}	0.0378	0.0752	0.0500
R_1 [$I > 2\sigma(I)$]	0.0566	0.0794	0.0375
wR_2 (all data)	0.1518	0.0806	0.0833

Table 2. Crystallographic data for **2-Sm** measured at different temperatures.

	2-Sm [433 K]	**2-Sm** [473 K]	**2-Sm** [473–293 K]
empirical formula	$C_{24}H_{21}C_{13}N_7Sm$	$C_{24}H_{21}C_{13}N_7Sm$	$C_{24}H_{22}C_{13}N_7OSm$
formula weight	664.18	664.18	681.19
space group	*P*31*c*	*P*31*c*	*P*31*c*
crystal system	hexagonal	hexagonal	hexagonal
a [Å]	11.5858(15)	11.5322(7)	11.5720(6)
b [Å]	11.5858(15)	11.5322(7)	11.5720(6)
c [Å]	13.0832(17)	12.9062(8)	13.1236(6)
γ [°]	120.00	120.00	120.00
V [Å^3]	1520.9(3)	1486.46(16)	1521.95(13)
Z	2	2	2
ρ_{calcd} [g cm^{-3}]	1.450	1.484	1.486
T [K]	433(2)	473(2)	298(2)
μ [mm^{-1}]	2.217	2.269	2.220
GOF	1.068	0.982	1.027
R_{int}	0.0584	0.0568	0.0544
R_1 [$I > 2\sigma(I)$]	0.0416	0.0301	0.0409
wR_2 (all data)	0.0810	0.0422	0.1069

Acknowledgements

This work was supported by the NSFC for Distinguished Young Scholars (20525310) and Innovative Groups (20821001), the 973 Program of China (2007CB815302), and the NSFC Projects 20773167 and 20731005.

[1] a) G. Férey, *Chem. Soc. Rev.* **2008**, *37*, 191–214; b) S. Kitagawa, R. Kitaura, S.-i. Noro, *Angew. Chem.* **2004**, *116*, 2388–2430; *Angew. Chem. Int. Ed.* **2004**, *43*, 2334–2375; c) C. Janiak, *Dalton Trans.* **2003**, 2781–2804; d) D. Bradshaw, J. B. Claridge, E. J. Cussen, T. J. Prior, M. J. Rosseinsky, *Acc. Chem. Res.* **2005**, *38*, 273–282; e) M. Eddaoudi, D. B. Moler, H.-L. Li, B.-L. Chen, T. M. Reineke, M. O'Keeffe, O. M. Yaghi, *Acc. Chem. Res.* **2001**, *34*, 319–330; f) M. P. Suh, Y. E. Cheon, E. Y. Lee, *Coord. Chem. Rev.* **2008**, *252*, 1007–1026; g) D. L. Long, R. J. Hill, A. J. Blake, N. R. Champness, P. Hub-

berstey, C. Wilson, M. Schröder, *Chem. Eur. J.* **2005**, *11*, 1384–1391; h) L. Pan, D. H. Olson, L. R. Ciemnolonski, R. Heddy, J. Li, *Angew. Chem.* **2006**, *118*, 632–635; *Angew. Chem. Int. Ed.* **2006**, *45*, 616–619; i) E. Coronado, J. R. Galán-Mascarós, C. J. Gómez-Garcia, V. Laukhin, *Nature* **2000**, *408*, 447–449; j) P. G. Lacroix, I. Malfant, S. Benard, P. Yu, E. Riviere, K. Nakatani, *Chem. Mater.* **2001**, *13*, 441–449; k) S. Karasawa, Y. Sano, T. Akita, N. Koga, T. Itoh, H. Iwamura, P. Rabu, M. Drilion, *J. Am. Chem. Soc.* **1998**, *120*, 10080–10087.

[2] a) K. Li, D. H. Olson, J. Y. Lee, W. Bi, K. Wu, T. Yuen, Q. Xu, J. Li, *Adv. Funct. Mater.* **2008**, *18*, 2205–2214; b) G. Férey, C. Mellot-Draznieks, C. Serre, F. Millange, *Acc. Chem. Res.* **2005**, *38*, 217–225; c) R. Kitaura, K. Seki, G. Akiyama, S. Kitagawa, *Angew. Chem.* **2003**, *115*, 444–447; *Angew. Chem. Int. Ed.* **2003**, *42*, 428–431; d) K. Hanson, N. Calin, D. Bugaris, M. Scancella, S. C. Sevov, *J. Am. Chem. Soc.* **2004**, *126*, 10502–10503; e) P. D. C. Dietzel, B. Panella, M. Hirscher, R. Blom, H. Fjellvåg, *Chem. Commun.* **2006**, 959–961; f) E. Y. Lee, S. Y. Jang, M. P. Suh, *J. Am. Chem. Soc.* **2005**, *127*, 6374–6381; g) L. G. Beauvais, M. P. Shores, J. R. Long, *J. Am. Chem. Soc.* **2000**, *122*, 2763–2772; h) Q.-R. Fang, G.-S. Zhu, Z. Jin, Y.-Y. Ji, J.-W. Ye, M. Xue, H. Yang, Y. Wang, S.-L. Qiu, *Angew. Chem.* **2007**, *119*, 6758–6762; *Angew. Chem. Int. Ed.* **2007**, *46*, 6638–6642; i) S. Ma, D. Sun, J. M. Simmons, C. D. Collier, D. Yuan, H.-C. Zhou, *J. Am. Chem. Soc.* **2008**, *130*, 1012–1016.

[3] a) L. J. Barbour, *Chem. Commun.* **2006**, 1163–1168; b) L. J. Murray, M. Dincă, J. R. Long, *Chem. Soc. Rev.* **2009**, *38*, 1294–1314; c) K. Biradha, A. Ramanan, J. J. Vittal, *Cryst. Growth Des.* **2009**, *9*, 2969–2970.

[4] a) G. Férey, C. Mellot-Draznieks, C. Serre, F. Millange, J. Dutour, S. Surblé, I. Margiolaki, *Science* **2005**, *309*, 2040–2042; b) M. Eddaoudi, J. Kim, N. Rosi, D. Vodak, J. Wachter, M. O'Keeffe, O. M. Yaghi, *Science* **2002**, *295*, 469–472; c) S. S.-Y. Chui, S. M.-F. Lo, J. P. H. Charmant, A. G. Orpen, I. D. Williams, *Science* **1999**, *283*, 1148–1150.

[5] a) S. Lim, H. Kim, N. Selvapalam, K.-J. Kim, S. J. Cho, G. Seo, K. Kim, *Angew. Chem.* **2008**, *120*, 3400–3403; *Angew. Chem. Int. Ed.* **2008**, *47*, 3352–3355; b) N. Malek, T. Maris, M.-È. Perron, J. D. Wuest, *Angew. Chem.* **2005**, *117*, 4089–4093; *Angew. Chem. Int. Ed.* **2005**, *44*, 4021–4025; c) T. Tanaka, T. Tasaki, Y. Aoyama, *J. Am. Chem. Soc.* **2002**, *124*, 12453–12462; d) K. Kobayashi, A. Sato, S. Sakamoto, K. Yamaguchi, *J. Am. Chem. Soc.* **2003**, *125*, 3035–3045.

[6] a) J. A. R. Navarro, E. Barea, M. A. Galindo, J. M. Salas, M. A. Romero, M. Quiros, N. Masciocchi, S. Galli, A. Sironi, B. Lippert, *J. Solid State Chem.* **2005**, *178*, 2436–2451; b) A. J. Fletcher, K. M. Thomas, M. J. Rosseinsky, *J. Solid State Chem.* **2005**, *178*, 2491–2510; c) G. K. H. Shimizu, *J. Solid State Chem.* **2005**, *178*, 2519–2526; d) K. Uemura, R. Matsuda, S. Kitagawa, *J. Solid State Chem.* **2005**, *178*, 2420–2429; e) C.-F. Zhuang, J. Y. Zhang, Q. Wang, Z.-H. Chu, D. Fenske, C.-Y. Su, *Chem. Eur. J.* **2009**, *15*, 7578–7585.

[7] a) S. Kitagawa, K. Uemura, *Chem. Soc. Rev.* **2005**, *34*, 109–119; b) D. Bradshaw, J. E. Warren, M. J. Rosseinsky, *Science* **2007**, *315*, 977–980; c) G. H. Halder, C. J. Kepert, B. Moubaraki, K. S. Murray, J. D. Cashion, *Science* **2002**, *298*, 1762–1765; d) D. N. Dybtsev, H. Chun, K. Kim, *Angew. Chem.* **2004**, *116*, 5143–5146; *Angew. Chem. Int. Ed.* **2004**, *43*, 5033–5036; e) J. P. Zhang, Y. Y. Lin, W. X. Zhang, X. M. Chen, *J. Am. Chem. Soc.* **2005**, *127*, 14162–14163; f) O. Ohmori, M. Kawano, M. Fujita, *J. Am. Chem. Soc.* **2004**, *126*, 16292–16295; g) C.-L. Chen, A. M. Goforth, M. D. Smith, C.-Y. Su, H.-C. Zur Loye, *Angew. Chem.* **2005**, *117*, 6831–6835; *Angew. Chem. Int. Ed.* **2005**, *44*, 6673–6677.

[8] a) S. K. Mäkinen, N. J. Melcer, M. Parvez, G. K. H. Shimizu, *Chem. Eur. J.* **2001**, *7*, 5176–5182; b) D. V. Soldatov, J. A. Ripmeester, *Chem. Eur. J.* **2001**, *7*, 2979–2994; c) D. V. Soldatov, G. D. Enright, J. A. Ripmeester, *Chem. Mater.* **2002**, *14*, 348–356; d) S. Takamizawa, E.-i. Nakata, H. Yokoyama, K. Mochizuki, W. Mori, *Angew. Chem.* **2003**, *115*, 4467–4470; *Angew. Chem. Int. Ed.* **2003**, *42*, 4331–4334; e) K. Takaoka, M. Kawano, M. Tominaga, M. Fujita, *Angew. Chem.* **2005**, *117*, 2189–2192; *Angew. Chem. Int. Ed.* **2005**, *44*, 2151–2154; f) G. J. Halder, C. J. Kepert, *J. Am. Chem. Soc.* **2005**, *127*, 7891–7900.

[9] a) D. D. MacNicol, J. J. McKendrick, D. R. Wilson, *Chem. Soc. Rev.* **1978**, *7*, 65–87; b) M. Miyata, M. Shibakami, S. Chirachanchai, K. Takemoto, N. Kasai, K. Miki, *Nature* **1990**, *343*, 446–447; c) A. T. Ung, D. Gizachew, R. Bishop, M. L. Scudder, I. G. Dance, D. C. Craig, *J. Am. Chem. Soc.* **1995**, *117*, 8745–8756; d) T. Dewa, K. Endo, Y. Aoyama, *J. Am. Chem. Soc.* **1998**, *120*, 8933; e) K. T. Holman, A. M. Pivovar, J. A. Swift, M. D. Ward, *Acc. Chem. Res.* **2001**, *34*, 107–118; f) J. L. Atwood, L. J. Barbour, A. Jerga, B. L. Schottel, *Science* **2002**, *298*, 1000–1002; g) L. R. Nassimbeni, *Acc. Chem. Res.* **2003**, *36*, 631–637; h) C. Trolliet, G. Poulet, A. Tuel, J. D. Wuest, P. Sautet, *J. Am. Chem. Soc.* **2007**, *129*, 3621–3626.

[10] a) K. Uemura, K. Saito, S. Kitagawa, H. Kita, *J. Am. Chem. Soc.* **2006**, *128*, 16122–16130; b) C. B. Aakeröy, A. M. Beatty, D. S. Leinen, *Angew. Chem.* **1999**, *111*, 1932–1936; *Angew. Chem. Int. Ed.* **1999**, *38*, 1815–1819; c) S. A. Dalrymple, G. K. H. Shimizu, *J. Am. Chem. Soc.* **2007**, *129*, 12114–12116; d) M. D. Stephensonn, M. J. Hardie, *CrystEngComm* **2007**, *9*, 496–502; e) A. M. Beatty, *Coord. Chem. Rev.* **2003**, *246*, 131–143.

[11] a) S. Tanase, M. Andruh, A. Müller, M. Schmidtmann, C. Mathonièrec, G. Rombautc, *Chem. Commun.* **2001**, 1084–1085; b) A. H. Mahmoudkhani, V. Langer, *Cryst. Growth Des.* **2002**, *2*, 21–25.

[12] G. P. Stahly, *Cryst. Growth Des.* **2007**, *7*, 1007–1026.

[13] a) B. Moulton, M. J. Zaworotko, *Chem. Rev.* **2001**, *101*, 1629–1658; b) H. G. Brittain, *J. Pharm. Sci.* **2007**, *96*, 705–728; c) G. R. Desiraju, *Cryst. Growth Des.* **2008**, *8*, 3–5.

[14] a) S. Liu, L. Getmini, A. J. Remg, R. C. Thompson, C. Orvig, *J. Am. Chem. Soc.* **1992**, *114*, 6081–6087; b) X.-P. Yang, C.-Y. Su, B.-S. Kang, X.-L. Feng, W.-L. Xiao, H.-Q. Liu, *J. Chem. Soc. Dalton Trans.* **2000**, 3253–3260.

[15] a) R. Taylor, O. Kennard, *J. Am. Chem. Soc.* **1982**, *104*, 5063–5070; b) G. A. Jeffrey, H. Maluszynska, *Int. J. Biol. Macromol.* **1982**, *4*, 173–185; c) J. A. Atwood, F. Hamada, K. D. Robinson, G. W. Orr, R. L. Vincent, *Nature* **1991**, *349*, 683–684.

[16] A. L. Spek, *J. Appl. Crystallogr.* **2003**, *36*, 7–13.

[17] a) T. K. Maji, K. Uemura, H.-C. Chang, R. Matsuda, S. Kitagawa, *Angew. Chem.* **2004**, *116*, 3331–3334; *Angew. Chem. Int. Ed.* **2004**, *43*, 3269–3272; b) F. Millange, C. Serre, N. Guillou, G. Férey, R. Walton. *Angew. Chem.* **2008**, *120, 4168–4173; Angew. Chem. Int. Ed.* **2008**, 47, 4100–4105; *Angew. Chem. Int. Ed.* **2008**, *47*, 4100–4105; c) R. Kitaura, G. Onoyama, H. Sakamoto, R. Matsuda, S. i. Noro, S. Kitagawa, *Angew. Chem.* **2004**, *116*, 2738–2741; *Angew. Chem. Int. Ed.* **2004**, *43*, 2684–2687.

[18] a) R. Kitaura, K. Fujimoto, SI. Noro, M. Kondo, S. Kitagawa, *Angew. Chem.* **2002**, *114*, 141–143; *Angew. Chem. Int. Ed.* **2002**, *41*, 133–135; b) K. Seki, *Phys. Chem. Chem. Phys.* **2002**, *4*, 1968–1971.

[19] a) D. Dybtsev, H. Chun, K. Kim, *Angew. Chem.* **2004**, *116*, 5143–5146; *Angew. Chem. Int. Ed.* **2004**, *43*, 5033–5036; b) C. D. Wu, W. Lin, *Angew. Chem.* **2005**, *117*, 1994–1997; *Angew. Chem. Int. Ed.* **2005**, *44*, 1958–1961; c) C. Yang, X. Wang, M. A. Omary, *Angew. Chem.* **2009**, *121*, 2538–2543; *Angew. Chem. Int. Ed.* **2009**, *48*, 2500–2505; d) T. K. Trung, P. Trens, N. Tanchoux, S. Bourrelly, P. L. Llewellyn, S. Loera-Serna, C. Serre, T. Loiseau, F. Fajula, G. Férey, *J. Am. Chem. Soc.* **2008**, *130*, 16926–16932.

[20] a) C. Piguet, A. F. Williams, G. Bernardinelli, E. Moret, J. C. G. Bünzli, *Helv. Chim. Acta* **1992**, *75*, 1697; b) M. Pan, X.-L. Zhang, Y. Liu, W.-S. Liu, C.-Y. Su, *Dalton Trans.* **2009**, 2157–2169; c) C.-Y. Su, B.-S. Kang, X.-Q. Mu, J. Sun, Y.-X. Tong, Z.-N. Chen, *Aust. J. Chem.* **1998**, *51*, 565–571.

[21] A. R. Oki, P. K. Bommarreddy, H. M. Zhang, N. Hosmane, *Inorg. Chim. Acta* **1995**, *231*, 109–114.

[22] SHELX 97, Program for Crystal Structure Solution and Refinement, G. M. Sheldrick, Göttingen University, Göttingen, **1997**.

Received: July 11, 2009
Published online: December 18, 2009

